MOLECULAR AND CELLULAR BIOLOGY, May 2005, p. 4229–4236 Vol. 25, No. 10
0270-7306/05/$08.00+0 doi:10.1128/MCB.25.10.4229–4236.2005

Targeted Disruption of the *Mn1* Oncogene Results in Severe Defects in Development of Membranous Bones of the Cranial Skeleton

Magda A. Meester-Smoor,[1] Marcel Vermeij,[1] Marjolein J. L. van Helmond,[1] Anco C. Molijn,[1]† Karel H. M. van Wely,[1]‡ Arnold C. P. Hekman,[1] Christl Vermey-Keers,[2] Peter H. J. Riegman,[1] and Ellen C. Zwarthoff[1]*

Department of Pathology, Josephine Nefkens Institute, Erasmus MC, Rotterdam, The Netherlands,[1] and Department of Plastic and Reconstructive Surgery, Erasmus MC, Rotterdam, The Netherlands[2]

Received 23 November 2004/Accepted 26 February 2005

Fusion of the *MN1* gene to *TEL* (*ETV6*) results in myeloid leukemia. The fusion protein combines the transcription activating domain of MN1 and the DNA binding domain of TEL and is thought to act as a deranged transcription factor. In addition, disruption of the large first exon of the *MN1* gene is thought to inactivate MN1 function in a meningioma. To further investigate the role of *MN1* in cancer, we generated *Mn1* knockout mice. *Mn1*$^{+/-}$ animals were followed for 30 months, but they had no higher incidence of tumor formation than wild-type littermates. *Mn1* null mice, however, were found to die at birth or shortly thereafter as the result of a cleft palate. Investigation of newborn or embryonic day 15.5 (E15.5) to E17.5 null mice revealed that the development of several bones in the skull was abnormal. The affected bones are almost exclusively formed by intramembranous ossification. They are either completely agenic at birth (alisphenoid and squamosal bones and vomer), hypoplastic, deformed (basisphenoid, pterygoid, and presphenoid), or substantially thinner (frontal, parietal, and interparietal bones). In heterozygous mice hypoplastic membranous bones and incomplete penetrance of the cleft palate were observed. We conclude that Mn1 is an important factor in development of membranous bones.

The *MN1* gene, localized on human chromosome 22, was cloned by our research group in 1995 as a candidate gene for sporadic meningioma, a benign brain tumor arising from the arachnoidal cap cells found on the surface coverings (called meninges) of the brain (12). In a meningioma, the *MN1* gene was found disrupted by a balanced translocation (4;22)(p16;q11). The breakpoint of the translocation lies within the first exon of the *MN1* gene, and the (truncated) protein was not detected. However, no mutations or deletions of the *MN1* gene were found in other meningiomas; thus the causative relationship between MN1 and meningiomas remains unclear. Subsequently, the *MN1* gene was found to play a role in acute myeloid leukemia (1). The translocation (12;22)(p13;q11) creates a fusion between the *MN1* and *TEL* (or *ETV6*) genes, resulting in the *MN1TEL* gene. The TEL protein is a member of the ETS family of transcription factors and contributes its C-terminal DNA binding domain (DBD) to the fusion protein MN1TEL. The MN1 protein donates 1,259 amino acids, 95% of its entire length, to the fusion protein. The fusion protein MN1TEL has transforming activity on NIH 3T3 cells and most likely acts as a deregulated transcription factor. MN1TEL may adhere to genes via the TEL moiety and activate these genes whereas they are normally controlled by the repressor TEL (2).

The MN1 gene comprises two exons and encodes a protein of 1,319 amino acids. The amino acid sequence shows no homology to other proteins or with specific domains with known functions. However, several proline/glutamine-rich regions and a polyglutamine stretch are present and point to a function in transcription regulation. We have shown previously that MN1 activates the transcription activity of the Moloney sarcoma virus long terminal repeat (MSV-LTR) and comprises multiple transcription activating domains (2). We recently determined that MN1 can act on the MSV-LTR (and other promoters) (unpublished results) as a transcription coactivator in retinoic acid receptor (RAR)-retinoic X receptor (RXR)-mediated transcription leading to a synergistic induction of expression when MN1 and the RAR-RXR ligand retinoic acid (RA) are combined. Furthermore, we have shown that there is an interplay between MN1 and P300 and RAC3, both known coactivators of retinoic acid receptors (24).

Hybridization of a cDNA probe to a blot containing DNA of a number of different species shows signals in species as evolutionarily distant as *Xenopus laevis* and *Drosophila melanogaster*, proving conservation of MN1 in evolution (12). The identity/similarity between human and murine MN1 proteins is 93%. Database searches reveal homologues of MN1 in mice (*Mus musculus*) and puffer fish (*Tetraodon nigroviridis*). The puffer fish MN1 homolog shows an identity/similarity of 64% with the human gene; the structure of the gene however is different. The gene consists of at least four exons; two additional small introns of 16 and 32 bp are present in the region covered by exon 1 in humans and mice. Surprisingly, in puffer fish, MN1 has less pronounced proline/glutamine-rich regions and lacks the large glutamine stretch (28Q) present in humans and mice halfway in the protein. The importance of the glutamine stretch is, however, underlined by the fact that the

* Corresponding author. Mailing address: Erasmus MC, Department of Pathology, Josephine Nefkens Institute, room Be300b, P.O. box 1738, 3000 DR Rotterdam, The Netherlands. Phone: 31 (0) 10 4087929. Fax: 31 (0) 10 4089487. E-mail: e.zwarthoff@erasmusmc.nl.

† Present address: Delft Diagnostic Laboratories, Delft, The Netherlands.

‡ Present address: Department of Immunology and Oncology, Centro Nacional de Biotechnologia, Madrid, Spain.

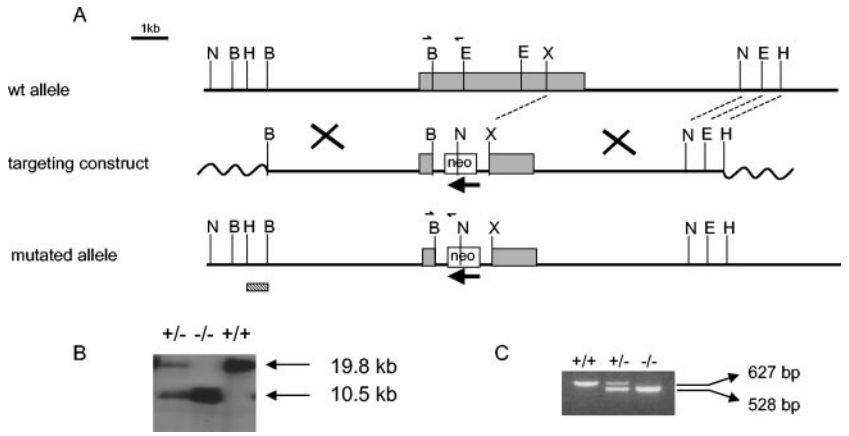

FIG. 1. Targeted disruption of the mouse *Mn1* gene. (A) Restriction enzyme map showing relevant sites (N, NcoI; B, BamHI; H, HindIII; E, EcoRI; X, XhoI) in the first exon of *Mn1* (top), the structure of the targeting vector (middle), and the targeted gene (bottom). The transcriptional orientation of the neomycin resistance gene (neo) is indicated with an arrow. The probe used for Southern blot hybridization, a 0.6-kb HindIII/BamHI fragment, is indicated as a hatched box. Primers are indicated with arrowheads. (B) Southern blot analysis of NcoI-digested genomic DNA of a mouse homozygous for the wild-type allele (+/+), a heterozygous mouse (+/−), and a mouse homozygous for the mutated allele (−/−). Wild-type (wt) and targeted alleles show bands of 19.8 and 10.5 kb, respectively, after hybridization with the indicated probe (hatched box). (C) PCR genotyping of mice using one forward primer and two reverse primers (sequences mentioned in Materials and Methods). The wt allele gives a band of 627 bp; the mutant product detected with the reverse primer located in the neomycin resistance gene is 528 bp.

puffer fish MN1 protein contains a large glutamine stretch (15Q) at a more N-terminal position, which is completely absent in humans and mice.

To determine the physiological significance of MN1 in vivo, we disrupted the *Mn1* gene in mice. The majority of heterozygous mice ($Mn1^{+/-}$) showed no obvious defects and appeared to have a normal life span and tumor incidence was not altered when compared to wild-type littermates. In *Mn1* null mice ($Mn1^{-/-}$) cranial bone development is severely affected with several bones being completely absent or hypoplastic. In addition, null mice have a cleft palate and, due to these defects, do not survive beyond day 1 after birth. A minor percentage of heterozygotes also die due to a cleft palate. Closer examination of $Mn1^{+/-}$ mice revealed that they have an intermediary deficiency in cranial bone formation.

MATERIALS AND METHODS

Construction of targeting vector. A cosmid clone was isolated from a C129 cosmid library (15) containing the mouse *Mn1* gene using human MN1 cDNA probe C (12). A BamHI/EcoRI fragment containing exon 1 was cloned in a targeting vector pMC1neo poly(A) (23). The neomycin resistance gene (*neo*) was inserted into exon 1 of the *Mn1* gene using BamHI/XhoI sites. The *neo* gene is controlled by the herpes simplex virus promoter, and the transcriptional orientation is opposite to the orientation of the *Mn1* gene (Fig. 1A).

Generation of $Mn1^{+/-}$ and $Mn1^{-/-}$ mice. The targeting vector was electroporated into strain 129 embryonic stem (ES) cells, and G418-resistant clones were isolated. G418-resistant clones were checked for the presence of the *neo* gene at the correct location using Southern blot hybridization on NcoI-digested DNA and a genomic probe upstream of the targeting construct. Targeted ES cells with correct integration of the *neo* gene and with the normal number of chromosomes (40) were injected into blastocysts of C57BL/6 mice. The blastocysts were injected into (strain FVB) foster mothers, and chimeras were obtained. Chimeric, transmitting males were crossed with normal FVB females for 10 generations to produce an inbred strain. Mice were genotyped by Southern blots or by PCR using three primers. Primer MuMn1-F (5′-CTTTGGGGGCA ACTTCGGTGG-3′) is a forward primer localized within exon 1 upstream of the inserted *neo* gene. Primer MuMn1-R (5′-CTCCAGACCCACAGGCATC-3′) is a reverse primer located in the part of exon 1 deleted by the integration of the *neo* gene and thus primes only on the wild-type *Mn1* allele, creating a 627-bp product in combination with MuMn1-F. The third primer is Neo-R (5′-GATG CAATGCGGCGGCTGCA-3′) and in combination with primer MuMN1-F detects the mutant allele resulting in a PCR product of 528 bp.

Examination of embryos, and newborn and adult mice: macroscopy, microscopy, and alizarin red/alcian blue staining. To obtain embryos of different stages of development (embryonic day 8.5 [E8.5] to E18.5), cesareans were performed on pregnant females. The day when a vaginal plug appeared was designated as E0.5. Extensive macroscopic and microscopic analysis was performed on embryos and newborn mice. Embryos were weighed and lung, heart, pancreas, spleen, liver, stomach, intestine, bladder, sex organs, thymus, and glands were dissected and macroscopically examined. They were fixed by immersion in 4% buffered formalin and embedded in paraffin. In addition, complete embryos were weighed, fixed, decalcified using EDTA for 5 days, and embedded in paraffin. Four-micrometer sections were deparaffinized in xylene, rehydrated, hematoxylin-eosin (HE) stained and microscopically examined. Alizarin red/alcian blue staining of complete embryos or newborn mice was performed using standard methods as described by Kaufman (10). Briefly, complete embryos were deskinned, and organs removed and fixed in 80% ethanol (EtOH; 2 days), dehydrated in 96% EtOH (2 days) followed by acetone (2 days), stained with alizarin red/alcian blue at 37°C for 2 days, and subsequently cleared using 1% KOH for several days. Finally, the specimens were stored in glycerol.

RESULTS

$Mn1^{+/-}$ mice have a normal life span. In order to generate *Mn1* knockout mice, a targeting construct was generated (Fig. 1A). Disruption of the *Mn1* gene at the BamHI site results in a truncated protein of 121 amino acids, deleting over 90% of the protein, including the transcription activating domain and the glutamine stretch. Chimeras successfully transmitted the targeted allele to the germ line, and after crossing, mice harboring only one functional *Mn1* gene were obtained ($Mn1^{+/-}$). Mice were genotyped using either Southern blot hybridization of NcoI-digested tail DNA (Fig. 1B) or by PCR using three primers simultaneously in one reaction (Fig. 1C). Because of the involvement of the *Mn1* gene in acute myeloid leukemia and its putative role in sporadic meningiomas, we determined whether the $Mn1^{+/-}$ genotype resulted in excess tumor formation or other forms of pathology. To this end, heterozygous males ($n = 143$) and females ($n = 95$) and wild-type siblings (127 males and 93 females) were followed for 30 months. No

TABLE 1. Genotyping of embryos of different embryonic stages

Embryonic stage	No. (%) of embryos with genotype:		
	+/+	+/−	−/−
E8.5	0	3	4
E10.5	4	11	1
E12.5	4	11	11
E14.5	4	8	4
E15.5	1	6	1
E16.5	4	2	3
E17.5	2	5	3
E18.5	3	5	8
Total	22 (20)	51 (47)	35 (32)

significant differences were observed in life span of $Mn1^{+/-}$ or $Mn1^{+/+}$ animals. Autopsies were performed on 47 $Mn1^{+/-}$ and 37 $Mn1^{+/+}$ animals that either died spontaneously or that were killed because of apparent lack of well-being. No significant differences in number of tumors between heterozygous or wild-type controls were observed. Macroscopic and microscopic examination of heart, lungs, kidney, spleen, liver, and muscle also revealed no abnormalities.

***Mn1* null mice and a minor percentage of *Mn1* heterozygotes die shortly after birth due to a cleft secondary palate.** Crosses between $Mn1^{+/-}$ mice failed to produce viable $Mn1^{-/-}$ mice. However, examination of embryos at various developmental stages (E8.5 to E18.5) showed that $Mn1^{-/-}$ mice were present in numbers compatible with normal Mendelian inheritance (Table 1). The $Mn1^{-/-}$ or $Mn1^{+/-}$ embryos of various developmental stages did not differ from their wild-type siblings in weight, length, and external appearance. These mice were examined microscopically, and no abnormalities were observed in any of the internal organs, including lung, heart, thymus, liver, kidney, pancreas, adrenal glands, and sex organs. Subsequently, a new series of breedings were closely monitored at the moment of delivery. A 10-h observation of newborn pups showed that a subset of pups died immediately following birth because they failed to start breathing, apparently because of breathing difficulties. A second group of pups did not suckle (empty stomachs), were lethargic, became cyanotic, and subsequently died. Genotyping of all dead pups showed that most of these pups (83%) are homozygous mutants. To our surprise, the remaining group of dead pups (17%) was genotyped as heterozygotes (Table 2). We first examined whether the lungs of the *Mn1* null mice displayed any abnormalities. Lungs of *Mn1* null mice and wild-type animals were examined by light and electron microscopy and were found to be normal (data not shown). Subsequently, total RNA was isolated from lungs of postnatal day 0 (P0) $Mn1^{-/-}$, $Mn1^{+/-}$, and wild-type animals. The mRNA levels of surfactants A, B, and C, factors known to be crucial for proper lung function, were analyzed using quantitative reverse transcription-PCR (RT-PCR) and again no differences were found (data not shown). Subsequently, a closer macroscopic examination of the head region of newborn mice revealed that all dead mice had a cleft secondary palate. In mice, this defect is not compatible with life. The cleft secondary palate was clearly visible on inferior views of the cranial base of the heads (Fig. 2A). Wild-type pups showed normal fusion of the palatal shelves while mutant mice do not. Three out of 21 (15%) heterozygotes also had a cleft secondary palate, but the defect was less severe when compared to null mice: the palatal shelves are closer to each other in the transversal direction leaving a cleft of only about half the distance when compared to homozygous *Mn1* knockouts. The palatal shelves in affected heterozygotes did form small rugae and were fused with the primary palate. Figures 2B and C show coronal sections of heads of newborn embryos at different positions. In wild-type animals the palate (p) has been formed

TABLE 2. Close examination of newborn pups

Status of newborn pups	No. (%) of pups of genotype:			Total (%)
	+/+	+/−	−/−	
Total	8 (18)	21 (48)	15 (34)	44 (100)
Viable	8	18	0	26
Dead[a]	0 (0)	3 (17)	15 (83)	18 (100)

[a] Pups either died directly after delivery or within the first 10 hours.

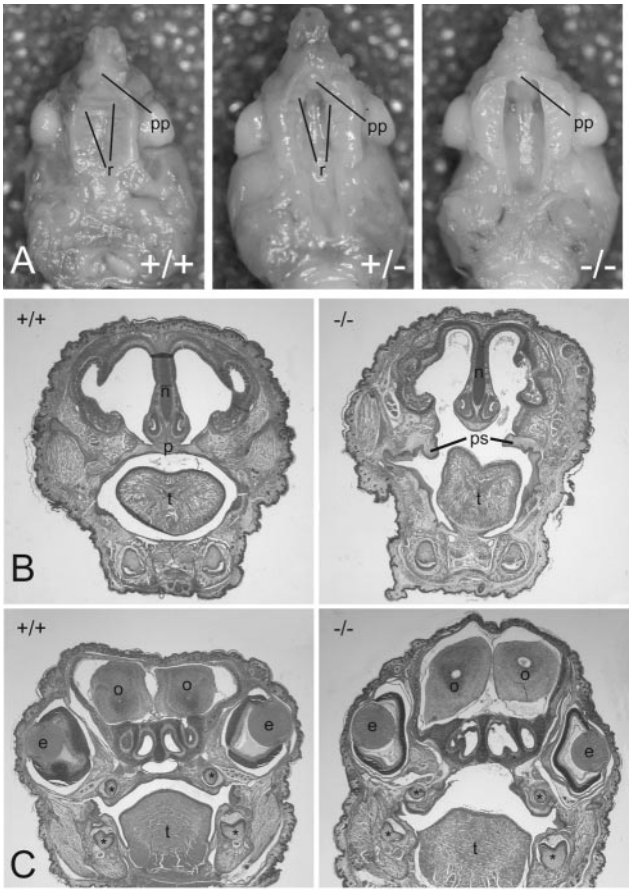

FIG. 2. Inferior views and histological sections of heads of newborn pups. (A) Normal palate with rugae (r) in a wild-type (wt; +/+) animal (left panel) and cleft secondary palate in $Mn1^{+/-}$ and $Mn1^{-/-}$ animals (middle and right panels). Small rugae on both sides of the cleft are seen in the heterozygote. pp, primary palate. (B and C) Coronal sections showing the correctly formed palate (p) in wt animals (left panels). Palatal shelves (ps) are not fused in $Mn1^{-/-}$ animals (right panels). Molars in maxilla and mandible are indicated with asterisks. e, eyes; o, olfactory lobe; n, nasal septum; t, tongue.

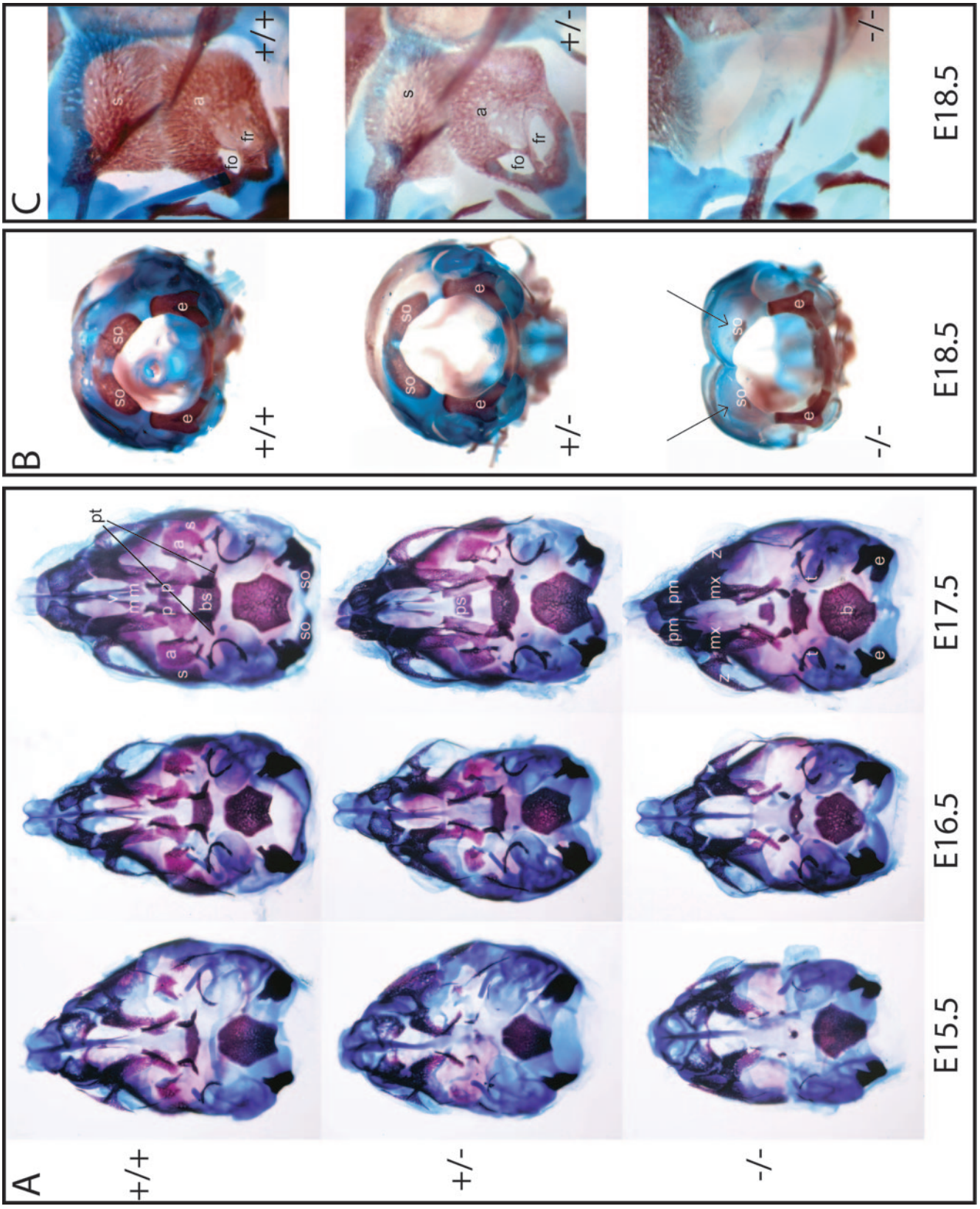
A
+/+
+/-
-/-
E15.5
E16.5
E17.5
pt
s
a
p
m
bs
so
ps
pm
mx
z
t
b
e
B
+/+
+/-
-/-
E18.5
so
e
C
+/+
+/-
-/-
E18.5
s
a
fo
fr

FIG. 3. Alizarin red/alcian blue staining of skulls. (A) Inferior views of skulls (mandibles removed) of E15.5, E16.5, and E17.5 mouse embryos. Wild-type (+/+), heterozygous *Mn1* (+/−), and homozygous *Mn1* (−/−) mice are shown in upper, middle, and lower panels, respectively. Within E17.5, the affected bones in $Mn1^{-/-}$ and $Mn1^{+/-}$ mice are indicated. In the E17.5 *Mn1* null mouse skull bones are indicated for orientation purposes. (B) Dorsal view of skulls of E18.5 mice showing the exoccipital and supraoccipital bones. Arrows indicate the delay in formation of the supraoccipital bone in the $Mn1^{-/-}$ mouse. (C) Detail of lateral view of E18.5 mice. The frontal direction of the skull is on the right side of the photographs, and the cranial base is on the bottom side of the photographs. Note the agenesis of alisphenoid and squamosal bone in the $Mn1^{-/-}$ mice. All animals of equal developmental stage are littermates. bs, basisphenoid; ps, presphenoid; p, palatine shelf; m, maxillary shelf; a, alisphenoid bone; pt, pterygoid bone; s, squamosal bone; so, supraoccipital bone; pm, premaxilla; z, zygomatic bone; mx, maxilla; t, tympanic ring; b, basioccipital bone; e, exoccipital bone; fo, foramen ovale; fr, foramen rotundum; v, vomer.

TABLE 3. Overview of bones within the skull of E18.5 Mn1 mice

Bone(s)	Result[a] for mice of genotype:	
	+/−	−/−
Maxilla	n	n
Mandible	n	n
Hard palate-maxillary	hy	hy
Hard palate-palatine	hy	hy
Premaxilla	n	n
Zygomatic	n	n
Squamosal	hy	ag
Tympanic ring	n	n
Frontal	n	hy
Pterygoid	hy	hy
Parietal	n	hy
Vomer	hy	ag
Interparietal	n	hy
Nasal bone	n	n
Supraoccipital	n	hy
Exoccipital	n	n
Alisphenoid	hy	ag
Basioccipital	n	n
Basisphenoid	hy	hy
Presphenoid	hy	hy
Maleus, incus, stapes	n	n

[a] n, normal development; hy, hypoplastic; ag, agenic.

correctly (Fig. 2B, left panel). In null mice ($Mn1^{-/-}$) the palatal shelves (ps) had developed (right panel of Fig. 2B) but were far apart and had not fused, resulting in a connection between the nasal and oral cavities. A cleft palate is frequently seen in mouse knockout models, and in some models this is accompanied by agenesis of molars (20, 22). In $Mn1^{-/-}$ mice, however, molars of both upper and lower jaw were correctly formed (Fig. 2C, left and right panels).

Skulls of mutant mice at E15.5 to E18.5 display many bone abnormalities. The process of palate formation is complex and depends on the correct position and formation of bone and soft tissue structures within the skull (21, 27). In order to visualize bone formation in the skull, wild-type, heterozygous and homozygous mice at different stages of development (E15.5 to E18.5) were deskinned and stained with alizarin red and alcian blue. Figure 3A shows inferior views of the skulls from which the mandibles were removed. At E15.5 the palatal shelves have just fused in wild-type mice ($Mn1^{+/+}$) and bone formation has taken place from both maxillary and palatine shelves. The increase in bone size within the palate is clearly visible at stage E16.5 (top, middle panel), and at stage E17.5 the bone structures from both sides had formed sutures (top, right panel). The $Mn1^{-/-}$ embryos had a cleft secondary palate, and the bone growth within the palatal shelves (both maxillary and palatine) is hypoplastic at all stages (Fig. 3A, bottom panels). Many additional abnormalities were obvious in the skulls of $Mn1^{-/-}$ mice. Several bone structures were absent (agenic) or were severely hypoplastic. In the E17.5, $Mn1^{+/+}$ skull, the alisphenoid (a) and squamosal (s) bones and the vomer (v) in a wild-type sibling are indicated. These bones were completely absent in the $Mn1^{-/-}$ mouse (Fig. 3A, bottom, −/−). Furthermore, the presphenoid (ps) and basisphenoid (bs) were hypoplastic and the pterygoid bones (pt) were not formed correctly. The heterozygous *Mn1* mice (Fig. 3A, middle panels) showed intermediate defects. In the palate, bone structures in both the

maxillary and palatine shelves are hypoplastic. In addition, bones that were agenic or hypoplastic in null mice (basisphenoid, alisphenoid, squamosal bones and vomer) were also clearly hypoplastic in *Mn1*$^{+/-}$ mice when compared to wild-type mice. The *Mn1*$^{+/-}$ mice of E15.5 and E16.5 had a closed palate; the *Mn1*$^{+/-}$ mouse of E17.5 had a cleft palate. These results show that the heterozygous *Mn1* mice display an intermediate phenotype when compared to *Mn1* null mice. This suggests that the extent of the defect may be related to dosage of the Mn1 protein.

We also stained heads of E18.5 mice to study the bone structures of the skull at a moment close to delivery. The dorsal view of the skull shows the normal development of the supraoccipital bone in a wild-type mouse (Fig. 3B, top). Bone formation starts in two ossification centers at E17, and fusion takes place at around P0. The formation of this bone in the *Mn1*$^{-/-}$ mouse is delayed (Fig. 3B, bottom). Heterozygous mice (+/−, middle panel) had a normally developing supraoccipital bone. Figure 3C shows a detail of the E18.5 skull in lateral view. The alisphenoid and squamosal bones were agenic in the *Mn1*$^{-/-}$ mouse (lower panel). The differences between wild type (+/+) and heterozygotes (+/−) at this stage were less pronounced, compared to differences seen at E15.5 and E16.5. At E18.5 the squamosal and alisphenoid bones were hypoplastic in heterozygotes (+/−) and the suture formation between these bones is in a less advanced stage. The bone within these structures is less dense, and the foramen ovale (for the mandibular nerve) and the foramen rotundum (for the maxillary nerve) are clearly larger, altogether indicating a delayed development of both bone structures in the *Mn1*$^{+/-}$ mouse. A closer look at the skulls of *Mn1* knockout mice and wild-type mice gave us the impression that all flat bones forming the roof of the skull (frontal, parietal and interparietal bones) were thinner in *Mn1*$^{-/-}$ mice. Staining of these bones was clearly less pronounced, and after processing the heads, the skulls from null mice appeared extremely fragile and compressible when compared to wild-type littermates. We performed micro-computerized tomography (CT) scans on skulls of wild-type and *Mn1* null mice (E18.5), and these confirm this observation: CT scans on skulls of a wild-type animal were readily obtained, but scans of skulls of *Mn1*$^{-/-}$ mice were of poor quality, because of very thin frontal, parietal, and interparietal bones (data not shown). A summary of all skull bones affected and not affected in *Mn1*$^{+/-}$ and *Mn1*$^{-/-}$ mice is shown in Table 3.

No abnormalities were observed in the appendicular skeleton, axial skeleton (below the skull), or internal organs of *Mn1*$^{-/-}$ and *Mn1*$^{+/-}$ mice. Skeletons of mice of different stages of embryonic development (E15.5 to E18.5) were stained with alizarin red/alcian blue, and close observation did not reveal any abnormalities besides the abnormalities in the skull. All limbs were formed correctly, and no delay of endochondral bone formation was observed in *Mn1*$^{-/-}$ or *Mn1*$^{+/-}$ compared to wild-type animals (data not shown). Analysis of *MN1* expression in human tissues showed that *MN1* is expressed in many tissues but at low levels with higher expression in skeletal muscle (12), kidney, and striatum (putamen and caudate nucleus) (unpublished results). The extensive analysis of many organs in the P0 *Mn1*$^{-/-}$ mice, however, revealed no abnormalities in these tissues or organs, indicating that *Mn1* plays no critical role in their development. Since *Mn1* null mice are not viable, the role of *Mn1* in normally functioning skeletal muscle, kidney, and striatum has not been investigated in this mouse model.

DISCUSSION

In this study we show that Mn1 plays a pivotal role in the development of membranous bones in the skull during embryogenesis. Agenesis is observed for the alisphenoid, and squamosal bones and vomer in null mice, the pterygoid, presphenoid, and basisphenoid bones are hypoplastic and the supraoccipital bone is delayed in formation. Furthermore, the parietal, frontal, and interparietal bones forming the roof of the skull are thinner and less mineralized. Bones not affected include the mandible, maxilla, and the nasal bones. In heterozygous *Mn1*$^{+/-}$ mice these developmental defects are less pronounced with normal mineralization of frontal, parietal, and interparietal bones of the skull and formation of the supraoccipital bone and the vomer. The squamosal and alisphenoid bones are formed but are hypoplastic and less mineralized and contain larger foramina. This suggests that there is a dosage effect of the Mn1 protein on cranial bone development. Incomplete penetrance is found for cleft secondary palate, a phenomenon seen in many mouse models with cleft secondary palate. Loss of one functional copy of the *Mn1* gene is compatible with a normal life span and does not lead to excess tumor formation or other pathologies.

Mineralization by osteoblasts occurs by two mechanisms: endochondral and intramembranous ossification (10). During endochondral ossification, precursor cells condense in areas destined to become bone, forming cartilage that will be replaced by bone material at a later stage. This mechanism is used for most of the vertebrate skeleton, including limbs, ribs, and part of the base of the skull. In the skull the parietal, interparietal, and frontal bones as well as the alisphenoid, pterygoid, squamosal, and palatal bones (from maxillary and palatine shelves) are formed by intramembranous ossification, which involves the condensation of precursor cells and the direct transition to differentiated bone cells, without an intermediate cartilage template formed (12). In mice, the remainder of the skull, including maxilla and mandible, is formed by a combination of the two processes. Thus nearly all bones affected in *Mn1*$^{-/-}$ mice are formed by the process of intramembranous ossification, and consequently it appears that *Mn1* plays a pivotal role in the formation of membranous bones during embryogenesis. The supraoccipital bone, which is delayed in its formation in *Mn1* null mice, is formed by endochondral ossification. The supraoccipital bone is formed late during embryonic development (E17.5), and processes involving the onset of bone formation are unknown. Possibly, the formation of bone structures in the vicinity of the supraoccipital bone, known to be affected in the *Mn1* knockout mice, influences the onset of ossification. The question remains whether all bone structures formed by intramembranous ossification are affected in *Mn1* null mice. The mandible and maxilla are formed by a combination of the two processes, and an impaired mineralization is difficult to detect in these structures by alizarin red/alcian blue stainings.

Since MN1 is able to function as a transcriptional coactiva-

tor, an interplay between MN1 and other transcription factors regulating intramembranous ossification is plausible. Many transcription factors known to have a function in bone formation, like *Cbf*-β, *Osx*, and *Runx*2 (11, 17, 18), are controlling osteoblast differentiation in both intramembranous and endochondral ossification. Cleidocranial dysplasia, an autosomal dominant skeletal disease in humans, is caused by mutations in the RUNX2 gene (16). Haploinsufficiency of the transcription factor causes skeletal abnormalities of both membranous and endochondral bones in patients, including enlarged calvaria with open fontanelles and short stature. Two isoforms of Runx2, I and II, have been found (26). Separate promoters control the expression of the two isoforms, resulting in two proteins with only minor differences in the N terminus. By generating selective *Runx2-II*-deficient mice, the separate functions of the two isoforms were studied. In *Runx2-II* null mice, intramembranous ossification was not affected, suggesting that it is the Runx2-I isoform that is responsible for proper development of membranous bones. Runx2-I and -II are subunits of the heterodimeric transcription factor PEBP2/CBF (25). The C-terminal region of Runx2 is involved in interaction with various transcription factors, coactivators, and corepressors. Since Mn1 is known to act as a transcriptional coactivator in RA-mediated transcription, it is possible that Mn1 acts as a coactivator in Runx2-I-related transcriptional regulation.

In humans no syndromes are known that resemble the abnormalities seen in *Mn1* knockout mice. Defects in membranous bones are rare; only two papers describe families with delayed intramembranous ossification (3, 6). During infancy, these patients show a complete lack of ossification of the calvarial bones forming the roof of the skull resulting in a soft skull. In adults, the cranial vault is ossified but is deformed because of delayed ossification. The temporalis (squamosal) and sphenoid bones are not severely affected and no cleft palate is observed in these patients. One of the families had a translocation (2;3)(p15;q12). The translocation breakpoints and the localization of *MN1* in the human genome (chromosome 22), together with the differences in defects observed, rule out the possibility that *MN1* is the mutated gene in these families. The gene mutated in these families may be involved only in intramembranous ossification of a subset of the calvarial bones forming the roof of the skull.

A short administration of RA to pregnant mice carrying embryos of E10 results in abnormalities showing similarities to the ones observed in *Mn1* knockout mice. At birth these mice show a failure of ossification at P0 of the parietal and interparietal bones and reduction in size of the alisphenoid and squamosal bones (8). Biochemical experiments in our group have shown that MN1 can act as a transcription coactivator in RAR-RXR-mediated transcription (24). Thus, since MN1 enhances RAR function, one would expect that obliteration of Mn1 has the opposite effect from a high, nonphysiological, dose of the RAR ligand RA. However, it is known that both long-term excess and deficiency of vitamin A in the diet of a pregnant mouse causes a broad range of abnormalities in the offspring (13, 14) and that the abnormalities in both diet conditions show great similarities. This shows that a shift in the balance of RAR-RXR-related processes results in similar defects. A more subtle short-term administration of RA at E10 or the lack of Mn1 also results in similar defects, indicative of an interplay between Mn1 and RA in the processes involving the correct formation of the affected bones.

Another mouse model showing striking similarities to the bone abnormalities observed in $Mn1^{-/-}$ mice is the $Dlx2^{-/-}$ mouse (20). *Dlx2* is a homeobox gene controlling the patterning of cells within the first and second proximal branchial arches starting around E8.5. Bones absent in the *Mn1* knockout mice are also agenic in the $Dlx2^{-/-}$ mice (squamosal and alisphenoid bones). Furthermore, both mouse models show abnormalities of basisphenoid and pterygoid bones, and a cleft of the secondary palate is observed in 80% of *Dlx2* knockout mice. However, there are also notable differences. The vomer is not affected in *Dlx2* knockout mice, and the supraoccipital bone is not delayed in formation. In addition, there is no evidence for impaired mineralization of parietal, frontal, and interparietal bones of the skull. In $Dlx2^{-/-}$ mice abnormalities in the inner ear, forebrain, and enteric nervous system are observed, but we have no evidence that any of these structures is affected in $Mn1^{-/-}$ mice. In conclusion, defects in $Mn1^{-/-}$ and $Dlx2^{-/-}$ mice overlap but there are also deficiencies associated with the lack of each gene separately.

The most obvious external abnormality observed in $Mn1^{-/-}$ mice and in a minor percentage of $Mn1^{+/-}$ mice is the cleft secondary palate. The formation of the palate is a complex process, and a cleft secondary palate has been observed in a number of transgenic mice (4, 7, 9, 13, 19, 20, 22) and in a spontaneous mutant mouse strain, the Twirler mice (5). Cleft secondary palate in these mice is caused by a variety of defects, including a deformed tongue ($Ryk^{-/-}$ mice) (7), shortened mandibles ($Msx1^{-/-}$ mice) (22), a wider midface (Twirler mice) (5), malformation of the inner ear region ($Hoxa\text{-}2^{-/-}$ mice) (4), agenesis of numerous bones of the lateral skull ($Dlx2^{-/-}$ mice) (20), and a failure to fuse the palatal shelves ($TGF\text{-}\beta3^{-/-}$ mice) (9, 19). Besides the *TGF*-β*3* knockout model, the palatal defects in these mice can be attributed, at least partially, to the malformations in the vicinity of the palatal shelves that cause mechanical hindrance in positioning, elevation, and fusion of the shelves. The cleft palate observed in $Mn1^{-/-}$ mice is most likely a secondary effect of missing bones in the vicinity of the palatal shelves, although we cannot rule out the possibility that Mn1 plays an intrinsic role in palatal development.

We conclude that loss of the *Mn1* gene is not compatible with life, that Mn1 plays an essential role in intramembranous bone formation, and that the lack of proper development of these parts of the cranial skeleton results in a cleft secondary palate. The *Mn1* knockout mouse is the first mouse model which selectively affects membranous bones and therefore presents an excellent model to study this complex process of bone formation.

ACKNOWLEDGMENTS

This work was supported by the Dutch Cancer Society (grant EUR1998-1778).

We thank H. Weinans and E. Waarsing from the Orthopaedic Research Laboratory, Erasmus MC, for performing micro-CT scans and N. Galjart, Department of Cell Biology, Erasmus MC, for the strain 129 cosmid library.

REFERENCES

1. **Buijs, A., S. Sherr, S. van Baal, S. van Bezouw, D. van der Plas, A. Geurts van Kessel, P. Riegman, R. Lekanne Deprez, E. Zwarthoff, A. Hagemeijer, et**

al. 1995. Translocation (12;22) (p13;q11) in myeloproliferative disorders results in fusion of the ETS-like TEL gene on 12p13 to the MN1 gene on 22q11. Oncogene **10:**1511–1519.
2. **Buijs, A., L. van Rompaey, A. C. Molijn, J. N. Davis, A. C. Vertegaal, M. D. Potter, C. Adams, S. van Baal, E. C. Zwarthoff, M. F. Roussel, and G. C. Grosveld.** 2000. The MN1-TEL fusion protein, encoded by the translocation (12;22)(p13;q11) in myeloid leukemia, is a transcription factor with transforming activity. Mol. Cell. Biol. **20:**9281–9293.
3. **Cargile, C. B., I. McIntosh, M. V. Clough, J. Rutberg, R. Yaghmai, B. K. Goodman, X. N. Chen, J. R. Korenberg, G. H. Thomas, and M. T. Geraghty.** 2000. Delayed membranous ossification of the cranium associated with familial translocation (2;3)(p15;q12). Am. J. Med. Genet. **92:**328–335.
4. **Gendron-Maguire, M., M. Mallo, M. Zhang, and T. Gridley.** 1993. Hoxa-2 mutant mice exhibit homeotic transformation of skeletal elements derived from cranial neural crest. Cell **75:**1317–1331.
5. **Gong, S. G., and R. L. Eulenberg.** 2001. Palatal development in Twirler mice. Cleft Palate Craniofac. J. **38:**622–628.
6. **Gonzalez-del Angel, A., A. Carnevale, and R. Takenaga.** 1992. Delayed membranous cranial ossification in a mother and child. Am. J. Med. Genet. **44:**786–789.
7. **Halford, M. M., J. Armes, M. Buchert, V. Meskenaite, D. Grail, M. L. Hibbs, A. F. Wilks, P. G. Farlie, D. F. Newgreen, C. M. Hovens, and S. A. Stacker.** 2000. Ryk-deficient mice exhibit craniofacial defects associated with perturbed Eph receptor crosstalk. Nat. Genet. **25:**414–418.
8. **Jiang, X., S. Iseki, R. E. Maxson, H. M. Sucov, and G. M. Morriss-Kay.** 2002. Tissue origins and interactions in the mammalian skull vault. Dev. Biol. **241:**106–116.
9. **Kaartinen, V., J. W. Voncken, C. Shuler, D. Warburton, D. Bu, N. Heisterkamp, and J. Groffen.** 1995. Abnormal lung development and cleft palate in mice lacking TGF-beta 3 indicates defects of epithelial-mesenchymal interaction. Nat. Genet. **11:**415–421.
10. **Kaufman, M. H.** 1992. The atlas of mouse development. Academic Press, London, United Kingdom.
11. **Kundu, M., A. Javed, J. P. Jeon, A. Horner, L. Shum, M. Eckhaus, M. Muenke, J. B. Lian, Y. Yang, G. H. Nuckolls, G. S. Stein, and P. P. Liu.** 2002. Cbfβ interacts with Runx2 and has a critical role in bone development. Nat. Genet. **32:**639–644.
12. **Lekanne Deprez, R. H., P. H. Riegman, N. A. Groen, U. L. Warringa, N. A. van Biezen, A. C. Molijn, D. Bootsma, P. J. de Jong, A. G. Menon, N. A. Kley, et al.** 1995. Cloning and characterization of MN1, a gene from chromosome 22q11, which is disrupted by a balanced translocation in a meningioma. Oncogene **10:**1521–1528.
13. **Lohnes, D., M. Mark, C. Mendelsohn, P. Dolle, A. Dierich, P. Gorry, A. Gansmuller, and P. Chambon.** 1994. Function of the retinoic acid receptors (RARs) during development. I. Craniofacial and skeletal abnormalities in RAR double mutants. Development **120:**2723–2748.
14. **Maden, M.** 2001. Vitamin A and the developing embryo. Postgrad. Med. J. **77:**489–491.
15. **Mazarakis, N., D. Michalovich, A. Karis, F. Grosveld, and N. Galjart.** 1996. Zfp-37 is a member of the KRAB zinc finger gene family and is expressed in neurons of the developing and adult CNS. Genomics **33:**247–257.
16. **Mundlos, S., F. Otto, C. Mundlos, J. B. Mulliken, A. S. Aylsworth, S. Albright, D. Lindhout, W. G. Cole, W. Henn, J. H. Knoll, M. J. Owen, R. Mertelsmann, B. U. Zabel, and B. R. Olsen.** 1997. Mutations involving the transcription factor CBFA1 cause cleidocranial dysplasia. Cell **89:**773–779.
17. **Nakashima, K., X. Zhou, G. Kunkel, Z. Zhang, J. M. Deng, R. R. Behringer, and B. de Crombrugghe.** 2002. The novel zinc finger-containing transcription factor osterix is required for osteoblast differentiation and bone formation. Cell **108:**17–29.
18. **Otto, F., A. P. Thornell, T. Crompton, A. Denzel, K. C. Gilmour, I. R. Rosewell, G. W. Stamp, R. S. Beddington, S. Mundlos, B. R. Olsen, P. B. Selby, and M. J. Owen.** 1997. Cbfa1, a candidate gene for cleidocranial dysplasia syndrome, is essential for osteoblast differentiation and bone development. Cell **89:**765–771.
19. **Proetzel, G., S. A. Pawlowski, M. V. Wiles, M. Yin, G. P. Boivin, P. N. Howles, J. Ding, M. W. Ferguson, and T. Doetschman.** 1995. Transforming growth factor-beta 3 is required for secondary palate fusion. Nat. Genet. **11:**409–414.
20. **Qiu, M., A. Bulfone, I. Ghattas, J. J. Meneses, L. Christensen, P. T. Sharpe, R. Presley, R. A. Pedersen, and J. L. Rubenstein.** 1997. Role of the Dlx homeobox genes in proximodistal patterning of the branchial arches: mutations of Dlx-1, Dlx-2, and Dlx-1 and -2 alter morphogenesis of proximal skeletal and soft tissue structures derived from the first and second arches. Dev. Biol. **185:**165–184.
21. **Ricks, J. E., V. M. Ryder, L. C. Bridgewater, B. Schaalje, and R. E. Seegmiller.** 2002. Altered mandibular development precedes the time of palate closure in mice homozygous for disproportionate micromelia: an oral clefting model supporting the Pierre-Robin sequence. Teratology **65:**116–120.
22. **Satokata, I., and R. Maas.** 1994. Msx1 deficient mice exhibit cleft palate and abnormalities of craniofacial and tooth development. Nat. Genet. **6:**348–356.
23. **Thomas, K. R., and M. R. Capecchi.** 1987. Site-directed mutagenesis by gene targeting in mouse embryo-derived stem cells. Cell **51:**503–512.
24. **van Wely, K. H., A. C. Molijn, A. Buijs, M. A. Meester-Smoor, A. J. Aarnoudse, A. Hellemons, P. den Besten, G. C. Grosveld, and E. C. Zwarthoff.** 2003. The MN1 oncoprotein synergizes with coactivators RAC3 and p300 in RAR-RXR-mediated transcription. Oncogene **22:**699–709.
25. **Wee, H. J., G. Huang, K. Shigesada, and Y. Ito.** 2002. Serine phosphorylation of RUNX2 with novel potential functions as negative regulatory mechanisms. EMBO Rep. **3:**967–974.
26. **Xiao, Z. S., A. B. Hjelmeland, and L. D. Quarles.** 2004. Selective deficiency of the "bone-related" Runx2-II unexpectedly preserves osteoblast-mediated skeletogenesis. J. Biol. Chem. **279:**20307–20313.
27. **Zhao, Y., Y. J. Guo, A. C. Tomac, N. R. Taylor, A. Grinberg, E. J. Lee, S. Huang, and H. Westphal.** 1999. Isolated cleft palate in mice with a targeted mutation of the LIM homeobox gene lhx8. Proc. Natl. Acad. Sci. USA **96:**15002–15006.